The DOI for this manuscript is doi: 10.1175/JAS-D-13-0154.1

# Midlatitude Tropopause and Low-Level Moisture

Yutian Wu *

Olivier Pauluis

*Courant Institute of Mathematical Sciences, New York University, New York, NY*

Submitted to J. Atmos. Sci. on May 24th 2013

Further Revised on October 11th, 2013



* *Corresponding author address:* Yutian Wu, Courant Institute of Mathematical Sciences, New York University, New York, NY, 10012

E-mail: yutian@cims.nyu.edu

## ABSTRACT

We propose a new relationship between the surface distribution of equivalent potential temperature and the potential temperature at the tropopause. Using a Gaussian approximation for the distribution of equivalent potential temperature, we argue that the tropopause potential temperature is approximately given by the mean equivalent potential temperature at the surface plus twice its standard derivation. This relationship is motivated by the comparison of the meridional circulation on dry and moist isentropes. It is further tested using four reanalysis datasets: the ERA-Interim Reanalysis, the NCEP/DOE Reanalysis II, the NCEP Climate Forecast System Reanalysis and the 20th Century Reanalysis version 2. The proposed relationship successfully captures the annual cycle of the tropopause, for both hemispheres. The results are robust among different reanalysis datasets albeit the 20th Century Reanalysis tends to over-estimate the tropopause potential temperature. Furthermore, the proposed mechanism also works well in obtaining the inter-annual variability (with climatological annual cycle removed) for Northern Hemisphere summer with above 0.6 correlation across different reanalyses. On the contrary, this mechanism is rather weak in explaining the inter-annual variability in the Southern Hemisphere and no longer works for Northern Hemisphere wintertime. This work suggests the important role of the moist dynamics in determining the midlatitude tropopause.

# 1. Introduction

The tropopause is usually defined as the transition region that separates the stably stratified stratosphere and the turbulent troposphere. It also corresponds to a sharp gradient in the concentration of various chemical constituents such as water vapor and ozone. As such, the location of tropopause is of fundamental importance for our understanding of the general circulation of the atmosphere. Held (1982) proposed a qualitative theory for the height of the tropopause and the tropospheric static stability by separating the dynamically constrained troposphere from the largely radiatively determined stratosphere. Assuming that the stratosphere is close to radiative equilibrium and the troposphere has a constant temperature lapse rate, one can obtain a radiative constraint between the height of the tropopause and the static stability of the troposphere. Provided a dynamical constraint relating the tropopause height and the tropospheric lapse rate, one is able to solve for these two quantities.

In the tropics, the dynamical constraint is relatively well understood and is given by the fact that the tropospheric lapse rate is close to moist adiabat due to the dominance of moist convection (Xu and Emanuel 1989). However, the dynamical constraint in the midlatitudes becomes difficult because of the role of the midlatitude eddies. There are two distinct perspectives for such dynamical constraint in the midlatitudes: one is based on dry baroclinic instability, and the other emphasizes the role of moist convection. Theories such as Stone (1978); Held (1982); Schneider (2004) belong to the first group, and relate the tropospheric static stability to the meridional temperature gradient based on the assumption that the atmosphere is in a state of near neutral stability for baroclinic instability: $\theta_z \sim \dfrac{f}{H\beta}\theta_y$, where $\theta$ is the potential temperature, $f$ and $\beta$ are the Coriolis parameter and its gradient, $H$ is some depth scale, and the subscripts z and y indicate the vertical and meridional derivatives, respectively.

A second perspective, presented in studies such as Emanuel (1988); Juckes (2000); Frierson et al. (2006); Frierson (2007); Korty and Schneider (2007); Frierson and Davis (2011);

Czaja and Blunt (2011), points to the importance of moist processes in the midlatitudes. For instance, Juckes (2000) proposes that the mean value of moist static stability ($\overline{\theta}_{ez}$, where $\theta_e$ is the equivalent potential temperature and the bar denotes time and zonal average) can be estimated as the sum of its minimum value and half the standard deviation of equivalent potential temperature. Then, by assuming that moist convection sets the minimum value of moist static stability to zero in the warm sector of the storms, the mean value of moist static stability is approximated as half the standard deviation of equivalent potential temperature, which is itself related to the meridional gradient of equivalent potential temperature: $\overline{\theta}_{ez} \sim \frac{1}{2}\overline{\theta_e'^2}^{1/2} \sim \overline{\theta}_{ey}$. This moist theory has been found to work substantially better than the dry theory in capturing the Southern Hemisphere annual cycle using the NASA Modern Era Retrospective-Analysis for Research and Applications (MERRA) reanalysis dataset (Frierson and Davis 2011) as well as predicting the extratropical static stability over a wide parameter range in both simple and comprehensive aquaplanet atmospheric general circulation model simulations (Frierson 2007).

Recently, Pauluis et al. (2008) and Pauluis et al. (2010) demonstrated the important role of moisture in the atmospheric general circulation, especially in the midlatitudes. They diagnosed the zonal mean atmospheric circulation in both $\theta$ and $\theta_e$ coordinates (respectively referred to as dry and moist isentropic circulation, hereafter) and found that both the two isentropic circulations exhibit a single equator-to-pole overturning cell in each hemisphere with poleward flow on high isentropic surfaces and equatorward flow on low isentropic surfaces. They noted that the moist circulation was stronger than its dry counterpart in the midlatitudes. It was further revealed that the larger circulation intensity averaged on moist isentropic surfaces is due to the better thermodynamic separation of the low-level poleward-moving warm moist air and the low-level equatorward-moving cold dry air, which, tend to cancel out each other in dry isentropic coordinate (Laliberté et al. 2012). The difference between the dry and moist isentropic circulation, defined as the moist recirculation, corresponds to the ascending branch of the midlatitude storm tracks that carries the low-level poleward-moving warm moist air into the upper troposphere lower stratosphere. This moist recirculation certainly connects the lower level of the atmosphere to the upper level via some dynamical processes. In this paper, we investigate the physical mechanisms underlying the moist recirculation process and eventually propose a dynamical constraint that relates the extratropical tropopause to the low-level equivalent potential temperature distribution.

This study is organized as follows: a theoretical development of the moist dynamical constraint is provided in section 2 and a description of the reanalysis datasets used in this study is given in section 3. Then, in section 4 the moist dynamical constraint is studied using an ensemble of reanalysis datasets. Section 5 concludes the paper.

# 2. Relationship Between Tropopause and Surface Equivalent Potential Temperature

## *a.* ***Dynamical Tropopause***

In the midlatitudes, the tropopause is often defined in terms of the distribution of the potential vorticity. The potential vorticity is given by $P = -g(\zeta + f)\dfrac{\partial\theta}{\partial p}$, where $\zeta$ is the vertical component of the relative vorticity and is about one order of magnitude smaller than the Coriolis parameter $f$ in the midlatitudes, and thus $P \approx -fg\dfrac{\partial\theta}{\partial p}$. The tropopause, regarded as the transition layer that separates low values of potential vorticity in the troposphere from large values in the stratosphere, is defined as the isentropic surface where the potential vorticity is equal to 2 PVU (potential vorticity unit, where 1 PVU is equal to $1.0 \times 10^{-6}$ K m$^2$ kg$^{-1}$ s$^{-1}$) (e.g., Holton et al. 1995). This dynamical tropopause definition works for regions away from the tropics and an example of the dynamical tropopause is shown in thick black dashed-dotted lines in Figure 1 away from 20°S and 20°N.

Other definitions of the tropopause, such as the thermal tropopause, in which the tropopause level is identified as the lowest level where the temperature lapse rate drops below 2 K/km (?), have been used. Such alternative definitions do not significantly affect the results, and, in the following, we will define the potential temperature at the tropopause $\theta_{\rm tp}$ as the mean potential temperature at which the potential vorticity is equal to 2 PVU, with the subscript tp denoting tropopause.

### *b.* ***Equivalent Potential Temperature in the Poleward Flow of Warm Moist Air***

Another determination of the tropopause is based on the mass flux of the atmospheric circulation and its isentropic streamfunction. The troposphere is relatively well-mixed by the action of weather system, with a short mixing time-scale on the order of one month. In contrast, mixing within the stratosphere is primarily the result of wave breaking and is much less efficient in general. One can thus think of the tropopause as the boundary between a region of fast overturning in the troposphere, and much slower overturning in the stratosphere. The isentropic streamfunction $\Psi(\phi, \theta)$, which is equal the net poleward mass flux for all air parcels across latitude $\phi$ whose potential temperature is less than $\theta$, thus provides a way to capture this overturning, and thus to determine the location of the tropopause. This is the argument used by Schneider (2004) who determined the tropopause as the potential temperature at which the (dry) isentropic streamfunction amounts to 10% of its maximum value.

The connection between the tropopause and isentropic streamfunction can be seen from Figure 1(a)(b), which shows the dry isentropic streamfunction using the ERA-Interim Reanalysis for December-January-February (DJF) and June-July-August (JJA), respectively. The streamfunction is constructed using the Statistical Transformed Eulerian Mean (to be discussed) that is largely similar to that of the exact calculation. In the extratropics, the dynamical tropopause generally overlaps with the dry isentropic surface corresponding to 10% of the maximum streamfunction, especially in Northern Hemisphere (NH) DJF and Southern Hemisphere (SH) JJA. However, it doesn't work well in NH JJA because of the very weak circulation there.

Here, we adopt a similar point of view and assume that the troposphere can be identified by the layer where most of the atmospheric meridional mass circulation takes place. Pauluis et al. (2008, 2010) have shown that approximately half of the global atmospheric circulation in the midlatitudes is associated with the poleward transport of warm, moist subtropical air near the surface, we consider the contribution of the surface flow to the moist isentropic circulation. In particular, we will determine the value of the equivalent potential temperature $\theta_{e,\mathrm{pf}}$ which accounts for 90% of the poleward mass flux of warm moist air near the surface, and postulate that $\theta_{e,\mathrm{pf}}$ offers a good estimate of the potential temperature at the tropopause, with the subscript pf denoting poleward flow. In doing so, we assume that the warm, moist air parcels in the low-level poleward-moving flow are able to rise more or less adiabatically to the tropopause within the storm tracks.

To determine $\theta_{e,\mathrm{pf}}$, we take advantage of the Statistical Transformed Eulerian Mean (STEM) introduced by Pauluis et al. (2011) which approximates the isentropic circulation by assuming a bivariate Gaussian distribution for the meridional mass transport. The STEM can accurately capture all the key features of the exact isentropic circulation with less than 10% error in the streamfunction. The STEM streamfunction for the moist isentropic circulation is the sum of the Eulerian-mean contribution and the eddy contribution, i.e.

$$
\begin{aligned}
\Psi_{\mathrm{STEM}}(\phi,\theta_e) &= \Psi_{\mathrm{eul}}(\phi,\theta_e) + \Psi_{\mathrm{eddy}}(\phi,\theta_e), && (1)\\
\Psi_{\mathrm{eul}}(\phi,\theta_e) &= \int_0^{p_s} \frac{2\pi a\cos\phi}{g}\overline{v}\frac{1}{2}\big[1+\mathrm{erf}\big(\frac{\theta_e-\overline{\theta_e}}{\sqrt{2\overline{\theta_e'^2}}^{1/2}}\big)\big]d\tilde{p}, && (2)\\
\Psi_{\mathrm{eddy}}(\phi,\theta_e) &= \int_0^{p_s} \frac{2\pi a\cos\phi}{g}\frac{-\overline{v'\theta_e'}}{\sqrt{2\pi\overline{\theta_e'^2}}^{1/2}}\exp\big(\frac{-(\theta_e-\overline{\theta_e})^2}{2\overline{\theta_e'^2}}\big)d\tilde{p}, && (3)
\end{aligned}
$$

where bars denote time and zonal averages, primes represent deviations from time and zonal averages, $\overline{v'\theta_e'}$ is the eddy flux of equivalent potential temperature and $\mathrm{erf}(x)$ is the error function, i.e. $\mathrm{erf}(x) = \frac{2}{\sqrt{\pi}}\int_0^x \exp(-x^2)dx$. While the Eulerian-mean component mainly represents the strong Hadley Cell in the tropics, the eddy component dominates in the midlatitudes. The dry isentropic circulation shown in Figure 1(a)(b) is also constructed using the STEM formulation by replacing $\theta_e$ with $\theta$.

We now determine $\theta_{e,\mathrm{pf}}$ as the value of the equivalent potential temperature at which the moist eddy streamfunction amounts to 10% of its maximum value:

$$\frac{|\Psi_{\mathrm{eddy}}(\phi, \theta_{e,\mathrm{pf}})|}{\max_{\theta_e} |\Psi_{\mathrm{eddy}}(\phi, \theta_e)|} = 0.1. \tag{4}$$

This definition assumes that 90% of the equatorward mass flux within the surface layer is balanced by the poleward mass flux taking place within the troposphere below the tropopause. Since the eddy flux of equivalent potential temperature maximizes in the lower troposphere near the surface, we assume it can be idealized as a delta function centered near the surface. According to Equation (3), the maximum of the moist eddy streamfunction ($\max_{\theta_e} |\Psi_{\mathrm{eddy}}(\phi, \theta_e)|$) is approximately achieved where the equivalent potential temperature equals the mean equivalent potential temperature near the surface. Therefore, the 10% of the maximum streamfunction, or where the tropopause is located, is reached where the equivalent potential temperature is approximately equal to the mean plus two standard deviations of the near surface equivalent potential temperature, i.e.,

$$\theta_{e,\mathrm{pf}} = \overline{\theta_{e,\mathrm{sfc}}} + 2\overline{\theta'^2_{e,\mathrm{sfc}}}^{1/2}, \tag{5}$$

and the subscript sfc refers to the value evaluated near the surface, where the eddy transport of equivalent potential temperature is the largest. For a Gaussian distribution, $\overline{\theta_e} + 2\overline{\theta'^2_e}^{1/2}$ corresponds to the 97.72nd percentile of the distribution and is a large and rare fluctuation of $\theta_e$.

Therefore, our main hypothesis here is that the potential temperature at the dynamical tropopause is directly tied to the equivalent potential temperature in the low-level poleward-moving warm, moist air, which, according to the STEM formulation, is approximately equal to the mean equivalent potential temperature plus twice its standard deviation:

$$\theta_{\mathrm{tp}} = \theta_{e,\mathrm{pf}} = \overline{\theta_{e,\mathrm{sfc}}} + 2\overline{\theta'^2_{e,\mathrm{sfc}}}^{1/2}. \tag{6}$$

In effect, Equation (6) implies that it is the large and rare fluctuation of low-level $\theta_e$ that rises more or less adiabatically to the tropopause level and modulates the tropopause potential temperature.

An example of the STEM moist isentropic circulation, based on the ERA-Interim Reanalysis dataset, is shown in Figure 1(c)(d). First of all, the moist isentropic circulation obtained using the STEM formulation is very similar to that of the exact calculation in both pattern and magnitude (not shown; similar results can be found in Figures 3-4 in Pauluis et al. (2011) using the NCEP/NCAR Reanalysis I). In the midlatitudes, the maximum of the STEM streamfunction is approximately reached as the equivalent potential temperature equals the mean equivalent potential temperature near the surface (shown in the middle thick gray line in Figure 1(c)(d)) and here the near surface value is estimated at 850 mb.

Two additional gray lines correspond to the mean surface equivalent potential temperature plus and minus twice the standard derivation, i.e. $\theta_{e,\mathrm{pf}} = \overline{\theta_{e,\mathrm{sfc}}} + 2\overline{\theta'^2_{e,\mathrm{sfc}}}^{1/2}$ and $\overline{\theta_{e,\mathrm{sfc}}} - 2\overline{\theta'^2_{e,\mathrm{sfc}}}^{1/2}$. Based on the previous arguments, 90% of the equatorward mass transport at low levels takes place between the lower and middle gray lines, while 90% of the poleward mass transport occurs between the middle and upper gray lines. The equatorward flow is indeed very well captured by this approach, and it is consistent with the findings of Held and Schneider (1999); Laliberté et al. (2013) who argued that the return flow in isentropic circulation should take place within isentropes that intersect the Earth's surface. The poleward flow is only partially captured by $\theta_{e,\mathrm{pf}}$ which overlaps with the 20-30% of the maximum streamfunction in the midlatitudes, under-estimating the equivalent potential temperature value of the 10% maximum streamfunction. This under-estimation is due to the fact that $\theta_{e,\mathrm{pf}}$ only accounts for the surface contribution of the eddy flux of equivalent potential temperature, omitting the contribution from the upper troposphere. It's worth noting that, in NH JJA, the moist circulation is much stronger than the dry counterpart and the difference is due to the latent heat transport associated with planetary-scale stationary eddies in the subtropics and transient eddies in the midlatitudes (see Figure 16 in Shaw and Pauluis 2012). While the dry isentropic surface corresponding to the 10% maximum streamfunction is poorly defined, the moist isentropic surface associated with the 10% maximum value is well defined and is reasonably well captured by the equivalent potential temperature of the low-level poleward-moving air flow $\theta_{e,\mathrm{pf}}$.

## 3. Reanalysis Datasets

Four reanalysis datasets are used to examine the robustness of the relationship described by Equation (6) including the ERA-Interim Reanalysis, the NCEP/DOE Reanalysis II, the NCEP Climate Forecast System Reanalysis, and the NOAA-CIRES 20th Century Reanalysis Version 2.

1. The ERA-Interim is the latest generation of the global atmospheric reanalysis produced by the European Centre for Medium-Range Weather Forecast (ECMWF) to replace the ERA-40 reanalysis (Dee and coauthors 2011). The ERA-Interim Reanalysis covers from 1979 to the present and has a horizontal resolution of T255 (0.75°longitude×0.75°latitude) with 60 model layers in the vertical and a model top at 0.1 mb. Significant progresses have been made relative to ERA-40 including the better representation of the hydrological cycle and the stratospheric circulation.

2. The second reanalysis dataset that is used in this study is the NCEP/DOE Reanalysis II (NCEP2) which covers from 1979 to the present (Kanamitsu et al. 2002). It has a horizontal resolution of T62 (2.5°longitude×2.5°latitude) and 28 vertical levels with a model top at about 3 mb.

3. The NCEP Climate Forecast System Reanalysis (CFSR) also covers from 1979 to the present and was designed as a global, high-resolution (both spatial and temporal) coupled atmosphere-ocean-land surface-sea ice system to provide the best estimate of the state of these coupled domains over the period (Saha and Coauthors 2010). The atmospheric component has a fine horizontal resolution of T382 (0.5°longitude×0.5°latitude, 2.5°longitude×2.5°latitude resolution is also available in the output and is used in this study), 64 levels in the vertical and a model top at 0.266 mb.

4. The 20th Century Reanalysis Version 2 (20CR) was recently produced by the National

Oceanic & Atmospheric Administration (NOAA) in collaboration with the Cooperative Institute for Research in Environmental Sciences (CIRES) and extends back to 1871 incorporating only surface pressure observations and prior estimates of sea surface temperature and sea-ice distributions (Compo and coauthors 2011). The long time range of this dataset allows the examination of decadal time scale climate processes such as the Pacific Decadal Oscillation and the Atlantic Multidecadal Oscillation. This reanalysis has a horizontal resolution of T62 (2°longitude×2°latitude) and 28 levels in the vertical with a model top at about 10 mb.

A short summary of these four reanalysis datasets is given in Table 1. Daily temperature and specific humidity during 1980-1999 from the above four reanalysis datasets are used in this study except for the CFSR where 6-hourly temperature and specific humidity are used. For the dynamical tropopause, the isentropic surface $\theta_{\mathrm{tp}}$ is identified where the 2 PVU potential vorticity surface is reached based on monthly averaged potential temperature and its pressure gradient. For the equivalent potential temperature of the low-level poleward-moving warm moist air flow, $\theta_{e,\mathrm{pf}}$ is evaluated at 850 mb and the results remain largely similar with the averages taken from 700 mb to 900 mb for the reanalyses (not shown).

# 4. Moist Dynamical Constraint in Reanalysis Datasets

In this section, we explore the proposed moist dynamical constraint in the midlatitudes using the four reanalysis datasets listed in section 3. Figure 1(c)(d) shows the climatology of the mean potential temperature evaluated at the dynamical tropopause $\theta_{\mathrm{tp}}$ (shown in thick black dashed-dotted lines) and also the mean value plus two standard deviations of the equivalent potential temperature distribution at 850 mb $\theta_{e,\mathrm{pf}}$ (shown in upper thick grey lines) for DJF and JJA, respectively, during 1980-1999 for the ERA-Interim Reanalysis dataset. The $\theta_{\mathrm{tp}}$ decreases from low to high latitudes and is consistent with the higher altitudes of the tropopause at low latitudes and the lower altitudes at high latitudes. Similarly $\theta_{e,\mathrm{pf}}$ at lower troposphere also decreases with latitudes, mainly following the decrease of the mean value of $\theta_e$ (not shown). The climatologies for both the low-level equivalent potential temperature and the tropopause potential temperature are largely consistent among the four reanalyses except for the 20th Century Reanalysis which tends to over-estimate the mean tropopause potential temperature (to be shown).

Furthermore, as shown in Figure 1(c)(d), there is some latitudinal shift between $\theta_{\mathrm{tp}}$ and $\theta_{e,\mathrm{pf}}$, with $\theta_{\mathrm{tp}}$ poleward of $\theta_{e,\mathrm{pf}}$. A latitudinal shift between the two quantities in the low and upper levels is physically reasonable because as the low-level poleward-moving warm moist air parcels ascend into the upper troposphere lower stratosphere, the air parcels also travel poleward. As the winter baroclinicity gets stronger, the poleward movement of the air parcels associated with moist convection is expected to be larger as compared to that of the summer where moist convection is more upright. This seasonality of the poleward shift can be seen in the NH, in which about 10 degrees of northward shift occur in DJF while a smaller northward shift takes place in JJA, especially between 40°N and 60°N. Without loss of generality, for all seasons and for both hemispheres, we focus on near surface $\theta_{e,\mathrm{pf}}$ at 30° latitude and tropopause $\theta_{\mathrm{tp}}$ at 40° latitude. This 10 degrees shift only helps to obtain similar $\theta_e$ values at lower and upper levels and is not crucial in capturing the annual cycle (to be discussed later).

### *a.* ***Annual Cycle***

Figure 2 shows the annual cycle of the moist dynamical constraint between the 850 mb $\theta_{e,\mathrm{pf}}$ at 30°N and the mean dynamical tropopause $\theta_{\mathrm{tp}}$ at 40°N for the four reanalysis datasets, including the ERA-Interim, the NCEP2, the NCEP CFSR, and the 20th Century Reanalysis, subdividing into different seasons. Both the correlation coefficient and linear regression coefficient are computed to better quantify the hypothesis. Consistent among different reanalyses, a very close to one correlation is found between the two quantities, i.e. above 0.98 for all four reanalyses. The results for the four reanalyses also lie in a straight line with close to one linear regression coefficient, i.e. 0.86-1.02. In particular, large values of tropopause

$\theta_{\rm tp}$ are found in NH summer (due to high tropopause altitudes), which is associated with large values of $\theta_{e,\rm pf}$ near the surface, while in NH winter, both $\theta_{\rm tp}$ and $\theta_{e,\rm pf}$ are relatively low. The results are in good agreement among different reanalysis datasets except for the 20th Century Reanalysis which produces values of $\theta_{e,\rm pf}$ similar to other reanalyses, but overestimates the mean tropopause $\theta_{\rm tp}$ values for all seasons, especially in NH summer (about 5 K larger than other three reanalyses at 40°N). Recalling that the 20th Century Reanalysis only assimilates surface pressure observations, possible errors at upper levels are, to some extent, within expectations. The annual cycle for the four reanalyses is summarized in Table 2 which includes the annual mean values for the $\theta_{e,\rm pf}$ at 30°N and the mean tropopause $\theta_{\rm tp}$ at 40°N as well as their correlation coefficient and linear regression coefficient for the annual cycle. The confidence intervals are constructed using the bootstrapping method by independently re-sampling the data points for a large number of times. Therefore, as shown in Figure 2, the proposed moist dynamical constraint successfully captures the annual cycle for NH extratropics.

Similarly for the SH, which is shown in Figure 3 and Table 3, the proposed hypothesis also works well in explaining the annual cycle with very close to one correlation coefficient (above 0.98) and close to one linear regression coefficient (about 0.7-0.8 for the four reanalyses). Note also that the amplitude of the annual cycle (winter-to-summer variation) is smaller in the SH than that in the NH, as expected. Again, the 20th Century Reanalysis has an over-estimation of the tropopause potential temperature, which occurs for all seasons.

The choice of 30° latitude for the lower troposphere and 40° latitude for the dynamical tropopause is not crucial in obtaining the annual cycle. Figure 4(a)(b) show the map of correlation and linear regression coefficient between $\theta_{e,\rm pf}$ and $\theta_{\rm tp}$ for a range of latitudinal points in the NH midlatitudes from 30°N to 60°N in the ERA-Interim Reanalysis. As shown, the correlation coefficient is always above 0.88 and the linear regression coefficient is always above 0.7 for this wide range of NH midlatitudes, and this is consistent among different reanalyses (not shown). At low-level 30°N and upper-level 40°N (highlighted in crosses), both the correlation coefficient and linear regression coefficient reach their maximum values approximately. The results are also shown for the SH midlatitudes from 30°S to 60°S (shown in Figure 4(c)(d)). The correlation coefficient is approximately maximized at low-level 30°S and upper-level 40°S; however, at these latitudes, the linear regression coefficient doesn't reach its maximum value.

### *b.* ***Inter-annual Variability***

We further explore whether the relationship between the low level equivalent potential temperature and the tropopause potential temperature can explain some of the inter-annual variability for the two hemispheres. The inter-annual variability here is identified as the monthly anomalies with monthly long-term averages removed. Figure 5 shows the monthly anomalies in $\theta_{\mathrm{tp}}$ at 40° latitude versus those in $\theta_{e,\mathrm{pf}}$ at 30° latitude for boreal summer (NH JJA) and austral summer (SH DJF), and the corresponding coefficients of correlation and linear regression. The results for the confidence intervals, constructed using the bootstrapping method, are shown in Table 4 and 5 for the NH and SH, respectively. For boreal summer, both the correlation coefficient and linear regression coefficient remain large and statistically significant for all the four reanalyses, i.e. above 0.6 in correlation and above 0.6 in linear regression. For austral summer, however, the correlation drops to 0.3-0.4 (small but still statistically significant) for majority of the reanalyses except for the 20th Century Reanalysis. Figure 6 shows the inter-annual variability but for boreal winter (NH DJF) and austral winter (SH JJA). Interestingly, while the results for SH JJA are similar to those in SH DJF with small correlation coefficients (i.e. about 0.2-0.3 in SH JJA), there is almost no correlation between the low levels and the upper levels in NH DJF. The above results suggest that the proposed moist dynamical constraint indeed applies in NH summer midlatitudes, even for monthly anomalies with climatological annual cycle removed. This moist dynamical constraint is rather weak in the SH and fails to work in NH DJF.

The coefficients of correlation and linear regression and their corresponding confidence intervals are also listed for spring and autumn in Table 4 and 5. The correlation is about 0.3-0.5 in boreal spring (NH MAM) for the four reanalyses while, in austral spring (SH SON), it's small and not significant in the ERA-Interim and NCEP2 reanalyses although the CFSR and the 20CR claim a significant correlation of about 0.4. In boreal and austral autumn (NH SON and SH MAM), both the correlation coefficient and linear regression coefficient are found to be significant and are about 0.3-0.4.

It's noted that the very close to one correlation coefficient for the annual cycle of the dynamical relationship, as shown in Figures 2 and 3, is largely due to the dominance of the annual cycle. However, in comparison to the previous work of Juckes 2000; Frierson et al. 2006; Frierson 2007; Frierson and Davis 2011, our proposed relationship achieves a higher correlation. Furthermore, the success in explaining the inter-annual variability in northern summer is indeed revealing (shown in Figure 5), which suggests the dominance of the moist dynamics in determining the monthly extratropical tropopause anomalies.

The distinct behaviors in NH summer and NH winter are, to some extent, within expectations. Although the annual cycle of the extratropical tropopause is largely determined by the annual cycle of the low-level eddy-induced fluctuations of equivalent potential temperature via midlatitude moist processes, the moist dynamics in the troposphere is not the only contributor to the extratropical tropopause. In fact, the inter-annual variability in stationary waves and in the stratospheric residual circulation is expected to be the strongest in boreal winter where the descending branch near the extratropical tropopause induces a strong adiabatic warming and tends to lower the tropopause (e.g., Birner 2010). It turns out that the stratospheric and tropospheric effects on the tropopause are opposite in sign (e.g., Birner 2010; Haqq-Misra et al. 2011), i.e. the tropospheric eddies always tend to stabilize the tropospheric lapse rate and lift the tropopause while the general tendency of the stratospheric eddies is to lower the extratropical tropopause which is strong in boreal winter and weak in boreal winter. Therefore, it's likely that in NH winter, the stratospheric influence may dominate the inter-annual variability. On the contrary, in NH summer, the stratospheric dynamical effect becomes minor and the tropopause is strongly controlled by the tropospheric dynamics.

### c. ***The Role of Moisture Variance***

Our analysis demonstrates a dynamical relationship between the low level distribution of equivalent potential temperature and the mean potential temperature at the tropopause in an ensemble of reanalysis datasets. The relationship in Equation (6) captures not only the annual cycle of the tropopause potential temperature, but also explains a large fraction of the inter-annual variability in NH summer. The quantity $\theta_{e,\mathrm{pf}}$, defined in Equation (5), corresponds to the 10% highest value of the equivalent potential temperature in the low-level poleward-moving warm, moist air. It depends not only on the mean value but also on the variance of $\theta_e$ near the surface. Through the annual cycle, the surface $\theta_{e,\mathrm{pf}}$ evolves greatly, but there is also a significant contribution from the variance itself. The eddy fluctuation of equivalent potential temperature is generally larger in summer than in winter and is about 15 K at 30° latitude in annual averages. In order to demonstrate the importance of the eddy-induced fluctuations of equivalent potential temperature, we compare the moist dynamical constraint with that using the mean value of $\theta_e$ plus a constant value of 15 K (in the absence of eddy fluctuations).

Figure 7 shows the comparison in NH annual cycle for the four reanalyses. The correlation coefficients are similar between the two measures and the coefficient of linear regression with the mean value of $\theta_e$ plus a constant is closer to one than that with the eddy fluctuations included. However, although the results for NH winter mostly overlap between the two measures, the moist dynamical constraint including the eddy contributions better captures the large values of the mean tropopause potential temperature in NH summer, consistent among the various reanalyses. This indicates that variances of low-level moisture and $\theta_e$ have a direct influence on the extratropical tropopause. In particular, the very high value of the potential temperature at the tropopause during the NH summer seems to be attributed in part to the very high value of the variance during that season. As this variance is due not only to the contribution of the midlatitude eddies, but also contains a significant contribution from differences between continental and oceanic regions, this would imply that a zonally symmetric model of the atmosphere would not be able to accurately reproduce the full range of tropopause height fluctuations. In fact, Shaw (2013) showed how planetary-scale transport can affect the tropopause in idealized aquaplanet model simulations and also discussed the importance of planetary-scale transport in the seasonal cycle.

# 5. Discussion and Conclusions

This study proposes a moist dynamical constraint for the midlatitudes that links the mean potential temperature value at the tropopause level to the equivalent potential temperature distribution in the lower troposphere. The constraint is motivated by previous analyses of the meridional circulation on moist isentropes which have shown that a large fraction of the global overturning circulation is tied to a poleward flow of warm, moist subtropical air that rises in the upper troposphere within the storm tracks (Pauluis et al. 2008, 2010). The constraint obtained here equates the 10th percentile of the equivalent potential temperature distribution in this poleward flow at low levels with the potential temperature of the tropopause. When the isentropic mass flux is estimated through the Statistical Transformed Eulerian Mean (STEM) framework (Pauluis et al. 2011), the 10th percentile of $\theta_e$ in the poleward flow is given by the mean surface equivalent potential temperature plus twice the standard deviation, i.e. $\theta_{e,\mathrm{pf}} = \overline{\theta_{e,\mathrm{sfc}}} + 2\overline{\theta'^2_{e,\mathrm{sfc}}}^{1/2}$ (Equation (5)). In effect, we assume that the poleward flow of warm, moist air rises to the tropopause within the storm tracks, and in doing so, sets the potential temperature at the tropopause, i.e $\theta_{\mathrm{tp}} = \theta_{e,\mathrm{pf}}$ (Equation (6)). Our approach thus emphasizes the role of moist ascent within the midlatitudes in determining the large-scale atmospheric circulation.

Four reanalysis datasets, the ERA-Interim Reanalysis, the NCEP/DOE Reanalysis II, the NCEP Climate Forecast System Reanalysis and the 20th Century Reanalysis version 2, are used in this study to test the relationship between the mean tropopause potential temperature and the low level equivalent potential temperature distribution. Here we summarize the findings:

- The proposed moist dynamical constraint is very successful in capturing the annual cycle of the tropopause. The correlation coefficient between the mean plus two standard deviations of the equivalent potential temperature in the lower troposphere and the mean potential temperature at the tropopause is very close to one. The results also lie in a straight line with a linear regression coefficient close to one. The above diagnostic results, which are robust among different reanalyses, suggest the important role of the moist processes associated with the baroclinic eddies in determining the large-scale atmospheric general circulation.

- At a given latitude, the tropopause potential temperature is somewhat warmer by a few degrees than the prediction based on the low level equivalent potential temperature distribution. This can be corrected by introducing a small poleward shift: in our analysis, we found that $\theta_{e,\mathrm{pf}}$ evaluated at 30° latitude very closely matches the tropopause potential temperature at 40° latitude for both hemispheres. Such poleward shift is smaller than the internal Rossby radius and is consistent with the physical interpretation of the low level flow of warm moist air being advected into the storm tracks.

- The moist dynamical constraint also works well in explaining the inter-annual variability in Northern Hemisphere summer, robust among different reanalysis datasets. The correlation coefficient for inter-annual variability is large in Northern Hemisphere summer (above 0.6), is quite small in the Southern Hemisphere (0.3-0.4), and drops to about zero in Northern Hemisphere winter. The difference between Northern Hemisphere summer and Northern Hemisphere winter suggests that the moist dynamics is more dominant in controlling the extratropical tropopause in summer while in winter the stratospheric large-scale dynamics is likely to play an important role.

This study demonstrates the important role of midlatitude moist processes in determining the large-scale atmospheric general circulation, in particular, where the tropopause is located. The midlatitude moist recirculation, known as the difference between dry and moist isentropic circulation, is found to be crucial in transporting energy and water vapor both upward and poleward and tends to lift the tropopause, i.e. in general, the stronger the moist recirculation, the higher the tropopause. This is clearly elucidated as the annual cycle of the extratropical tropopause is successfully captured by the low-level large and rare fluctuations of equivalent potential temperature. The dynamical mechanisms underlying the moist recirculation is not limited to warm conveyor belt which is a mesoscale phenomenon associated with midlatitude eddies (e.g., Eckhardt et al. 2004). Ascent of warm moist air flow can also be tied to deep convection over the continents (Shaw and Pauluis 2012) and more generic slantwise convection (Emanuel 1988). Our analysis finds that the best match occurs when the tropopause potential temperature is about 10° poleward of the near surface equivalent potential temperature. This indicates that the dynamical process connecting the lower and upper level of the atmosphere takes place over a relatively small horizontal scale, on the order of Rossby radius.

The proposed relationship is conceptually similar to the work of Juckes (2000); Frierson et al. (2006); Frierson (2007); Frierson and Davis (2011) albeit there are quantitative differences in that our analysis focuses on the relationship between the low level moisture distribution and the tropopause temperature rather than stratification. In Frierson and Davis (2011), they found that the moist scaling theory $\overline{\theta}_{ez} \sim \overline{\theta}_{ey}$ works well to explain the SH seasonal cycle (with correlation of 0.87) but performs less well in the NH (with correlation of 0.70). Our relationship achieves a higher correlation coefficient for both hemispheres. A key difference between Frierson and Davis (2011) and our analysis, lies in their assumption that the variance of equivalent potential temperature is proportional to the meridional gradient of $\theta_e$. In contrast, we use the variance computed from the Reanalysis datasets. As large portion of this variance is tied to stationary eddies and land-sea contrast, it is likely that a simple mixing length hypothesis underlying the scaling of Juckes (2000); Frierson and Davis (2011) is insufficient to explain the variance. This would imply that a more complete theory for the midlatitude stratification should include the effects of stationary waves and land-sea contrast. In fact, Shaw and Pauluis (2012) showed that the planetary-scale stationary waves of subtropical anticyclones and monsoons dominate the atmospheric meridional moisture transport in the subtropics during NH summer. In addition, Shaw (2013) further demonstrated the important role of low-level planetary-scale eddy transport in the seasonal cycle of the atmospheric general circulation including the height of the tropopause. In our work, the moist processes responsible for the annual cycle and inter-annual variability of the extra-tropical tropopause could be complex. And they are likely combined effects of subtropical anticyclones and monsoons, warm conveyor belts, slantwise moist convection and so on.

Our results strongly support the notion that the midlatitude stratification is directly affected by moist processes. This offers a strong challenge to the dry perspective that argues that the midlatitude stratification is determined primarily by (dry) baroclinic instability (Stone 1978; Schneider 2004). However, although the dry and moist perspectives on the height of the tropopause and the tropospheric static stability have different dynamical interpretations, they are not mutually exclusive. Indeed, a framework that relates the midlatitude stratification to both the meridional temperature gradient and low level humidity distribution, amounts in effect to prescribing the relative humidity distribution. Such joint interpretation would view the midlatitude eddies as simultaneously setting the stratification and controlling the subtropical water vapor distribution.

*Acknowledgments.*

The authors are grateful to helpful discussions with Profs. Tiffany A. Shaw, Edwin Gerber, Anthony D. Del Genio and Andy Majda. Olivier Pauluis and Yutian Wu have been supported by the NSF under Grant AGS-0944058 for this work. The 20th Century

Reanalysis V2 data provided by the NOAA/OAR/ESRL PSD, Boulder, Colorado, USA, from their Web site at http://www.esrl.noaa.gov/psd/.

# REFERENCES


Birner, T., 2010: Residual circulation and tropopause structure. *J. Atmos. Sci.*, **67(8)**, 2582–2600.

Compo, G. P. and coauthors, 2011: The Twentieth Century Reanalysis Project. *Quart. J. Roy. Meteor. Soc.*, **137**, 1–28.

Czaja, A. and N. Blunt, 2011: A new mechanism for oceancatmosphere coupling in midlatitudes. *Q. J. R. Meteorol. Soc.*, **137**, 1095–1101. doi: 10.1002/qj.814.

Dee, D. P. and coauthors, 2011: The ERA-Interim reanalysis: Configuration and performance of the data assimilation system. *Quart. J. R. Meteorol. Soc.*, **137**, 553–597.

Eckhardt, S., A. Stohl, H. Wernli, P. James, C. Forster, and N. Spichtinger, 2004: A 15-year climatology of warm conveyor belts. *J. Clim.*, **17**, 218–237.

Emanuel, K. A., 1988: Observational evidence of slantwise convective adjustment. *Mon. Wea. Rev.*, **116**, 1805–1816.

Frierson, D. M. W., 2007: Midlatitude static stability in simple and comprehensive general circulation models. *J. Atmos. Sci.*, **65(3)**, 1049–1062.

Frierson, D. M. W. and N. A. Davis, 2011: The seasonal cycle of midlatitude static stability over land and ocean in global reanalyses. *Geophys. Res. Lett.*, **38**, L13 803, doi:10.1029/2011GL047 747.

Frierson, D. M. W., I. M. Held, and P. Zurita-Gotor, 2006: A gray-radiation aquaplanet moist GCM. Part I: Static stability and eddy scale. *J. Atmos. Sci.*, **63(10)**, 2548–2566.

Haqq-Misra, J., S. Lee, and D. M. W. Frierson, 2011: Tropopause structure and the role of eddies. *J. Atmos. Sci.*, **68**, 2930–2944.

Held, I. and T. Schneider, 1999: The surface branch of the zonally averaged mass transport circulation in the troposphere. *J. Atmos. Sci.*, **56**, 1688–1697.

Held, I. M., 1982: On the height of the tropopause and the static stability of the troposphere. *J. Atmos. Sci.*, **39**, 412–417.

Holton, J. R., P. H. Haynes, M. E. McIntyre, A. R. Douglass, R. B. Rood, and L. Pfister, 1995: Stratosphere-troposphere exchange. *Rev. Geophys.*, **33**, 403–440.

Juckes, M. N., 2000: The static stability of the midlatitude troposphere: the relevance of moisture. *J. Atmos. Sci.*, **57**, 3050–3057.

Kanamitsu, M., W. Ebisuzaki, J. Woollen, S.-K. Yang, J. J. Hnilo, M. Fiorino, and G. L. Potter, 2002: NCEP-DOE AMIP-II Reanalysis (R-2). *Bull. Amer. Meteor. Soc.*, **83**, 1631–1643.

Korty, R. L. and T. Schneider, 2007: A climatology of the tropospheric thermal stratification using saturation potential vorticity. *J. Clim.*, **20**, 5977–5991.

Laliberté, F., T. A. Shaw, and O. Pauluis, 2012: Moist recirculation and water vapor transport on dry isentropes. *J. Atmos. Sci.*, **69**, 875–890.

Laliberté, F., T. A. Shaw, and O. Pauluis, 2013: A theory for the lower tropospheric structure of the moist isentropic circulation. *J. Atmos. Sci.*, **70**, 843–854.

Pauluis, O., A. Czaja, and R. Korty, 2008: The global atmospheric circulation on moist isentropes. *Sci.*, **321**, 1075–1078, doi:10.1126/science.1159 649.

Pauluis, O., A. Czaja, and R. Korty, 2010: The global atmospheric circulation in moist isentropic coordinates. *J. Clim.*, **23**, 3077–3093.

Pauluis, O., T. A. Shaw, and F. Laliberté, 2011: A statistical generalization of the transformed Eulerian-mean circulation for an arbitrary vertical coordinate system. *J. Atmos. Sci.*, **68**, 1766–1783.

Saha, S. and Coauthors, 2010: The NCEP Climate Forecast System Reanalysis. *Bull. Amer. Meteor. Soc.*, **91**, 1015–1057.

Schneider, T., 2004: The tropopause and the thermal stratification in the extratropics of a dry atmosphere. *J. Atmos. Sci.*, **61(12)**, 1317–1340.

Shaw, T. A., 2013: On the role of planetary-scale waves in the abrupt seasonal transition of the Northern Hemisphere general circulation. *J. Atmos. Sci.*, submitted.

Shaw, T. A. and O. Pauluis, 2012: Tropical and subtropical meridional latent heat transports by disturbances to the zonal mean and their role in the general circulation. *J. Atmos. Sci.*, **69**, 1872–1889.

Stone, P. H., 1978: Baroclinic adjustment. *J. Atmos. Sci.*, **35**, 561–571.

Xu, K.-M. and K. A. Emanuel, 1989: Is the tropical atmosphere conditionally unstable? *Mon. Wea. Rev.*, **117**, 1471–1479.

TABLE 1. The reanalysis datasets used in this study and their horizontal resolution for the atmospheric component.

| Reanalysis | Institution | Atmospheric Resolution (longitude$\times$latitude) |
|---|---|---|
| ERA-Interim | ECMWF | T255 ($0.75^\circ \times 0.75^\circ$) L60 |
| NCEP2 | NCEP/DOE | T62 ($2.5^\circ \times 2.5^\circ$) L28 |
| CFSR | NCEP | T382 ($0.5^\circ \times 0.5^\circ$) L64 |
| 20CR | NOAA/CIRES | T62 ($2^\circ \times 2^\circ$) L28 |

TABLE 2. The annual mean values for $\theta_{e,\mathrm{pf}}$ $(= \overline{\theta_e} + 2\overline{\theta_e'^2}^{1/2})$ at 850 mb at 30°N and the dynamical tropopause $\theta_{\mathrm{tp}}$ at 40°N, and their correlation coefficient and linear regression coefficient for the annual cycle for the four reanalysis datasets listed in Table 1. The corresponding confidence intervals are also shown and are constructed using the bootstrapping method by independently re-sampling the data points for a large number of times. Here the confidence interval is indicated by the mean value plus minus two standard deviations after bootstrapping.

| | Annual Mean $\theta_{e,\mathrm{pf}}$ at 850mb [K] | Mean Tropopause $\theta_{\mathrm{tp}}$ [K] | Correlation | Linear Regression |
|---|---|---|---|---|
| ERA-Interim | 333.74±1.33 | 333.66±1.16 | 0.986±0.003 | 0.863±0.019 |
| NCEP2 | 334.37±1.21 | 334.15±1.16 | 0.984±0.004 | 0.944±0.021 |
| CSFR | 332.39±1.23 | 334.25±1.19 | 0.985±0.003 | 0.952±0.021 |
| 20CR | 333.15±1.25 | 337.56±1.30 | 0.988±0.003 | 1.02±0.019 |

TABLE 3. Same as Table 2 but for the Southern Hemisphere with $\theta_{e,\mathrm{pf}}$ evaluated at 30°S and $\theta_{\mathrm{tp}}$ at 40°S.

| | Annual Mean $\theta_{e,\mathrm{pf}}$ at 850mb [K] | Mean Tropopause $\theta_{\mathrm{tp}}$ [K] | Correlation | Linear Regression |
|---|---|---|---|---|
| ERA-Interim | 328.23±0.94 | 330.64±0.74 | 0.982±0.004 | 0.771±0.019 |
| NCEP2 | 329.00±0.87 | 332.36±0.67 | 0.982±0.004 | 0.764±0.020 |
| CFSR | 326.84±0.85 | 331.37±0.72 | 0.981±0.004 | 0.831±0.021 |
| 20CR | 327.25±0.83 | 333.94±0.65 | 0.986±0.003 | 0.767±0.016 |

TABLE 4. The correlation coefficient and linear regression coefficient (shown in italics) between the monthly anomalies of 850 mb $\theta_{e,\mathrm{pf}}$ $(= \overline{\theta_e} + 2\overline{\theta_e'^2}^{1/2})$ at 30°N and those of the mean dynamical tropopause $\theta_{\mathrm{tp}}$ at 40°N, as well as their corresponding confidence intervals, for different seasons. Results of statistical significance are marked in bold.

| | NH Jun-Jul-Aug (JJA) | NH Dec-Jan-Feb (DJF) | NH Mar-Apr-May (MAM) | NH Sep-Oct-Nov (SON) |
|---|---|---|---|---|
| ERA-Interim | **0.652±0.141** | -0.068±0.317 | **0.516±0.226** | **0.369±0.242** |
| | ***0.769±0.217*** | *-0.097±0.465* | ***0.513±0.247*** | ***0.381±0.256*** |
| NCEP2 | **0.605±0.168** | -0.110±0.262 | **0.528±0.205** | **0.351±0.227** |
| | ***0.659±0.221*** | *-0.142±0.343* | ***0.476±0.177*** | ***0.393±0.264*** |
| CFSR | **0.606±0.162** | -0.016±0.284 | **0.388±0.372** | **0.354±0.216** |
| | ***0.626±0.197*** | *-0.023±0.420* | ***0.372±0.278*** | ***0.380±0.274*** |
| 20CR | **0.675±0.146** | 0.268±0.268 | **0.430±0.223** | **0.452±0.192** |
| | ***0.650±0.166*** | *0.334±0.337* | ***0.345±0.155*** | ***0.401±0.181*** |

TABLE 5. Same as Table 4 but for the Southern Hemisphere with $\theta_{e,\mathrm{pf}}$ evaluated at 30°S and $\theta_{\mathrm{tp}}$ at 40°S.

| | SH Jun-Jul-Aug (JJA) | SH Dec-Jan-Feb (DJF) | SH Mar-Apr-May (MAM) | SH Sep-Oct-Nov (SON) |
|---|---|---|---|---|
| ERA-Interim | **0.267±0.198** | **0.331±0.266** | **0.329±0.234** | 0.159±0.254 |
| | ***0.251±0.205*** | ***0.278±0.235*** | ***0.263±0.208*** | *0.160±0.272* |
| NCEP2 | **0.262±0.205** | **0.402±0.236** | **0.414±0.216** | 0.216±0.243 |
| | ***0.259±0.223*** | ***0.400±0.257*** | ***0.328±0.190*** | *0.203±0.239* |
| CFSR | 0.232±0.242 | **0.447±0.192** | **0.349±0.188** | **0.403±0.254** |
| | *0.292±0.338* | ***0.399±0.207*** | ***0.327±0.171*** | ***0.436±0.273*** |
| 20CR | **0.393±0.208** | **0.675±0.160** | **0.528±0.171** | **0.499±0.176** |
| | ***0.335±0.211*** | ***0.461±0.130*** | ***0.356±0.159*** | ***0.410±0.202*** |

# List of Figures

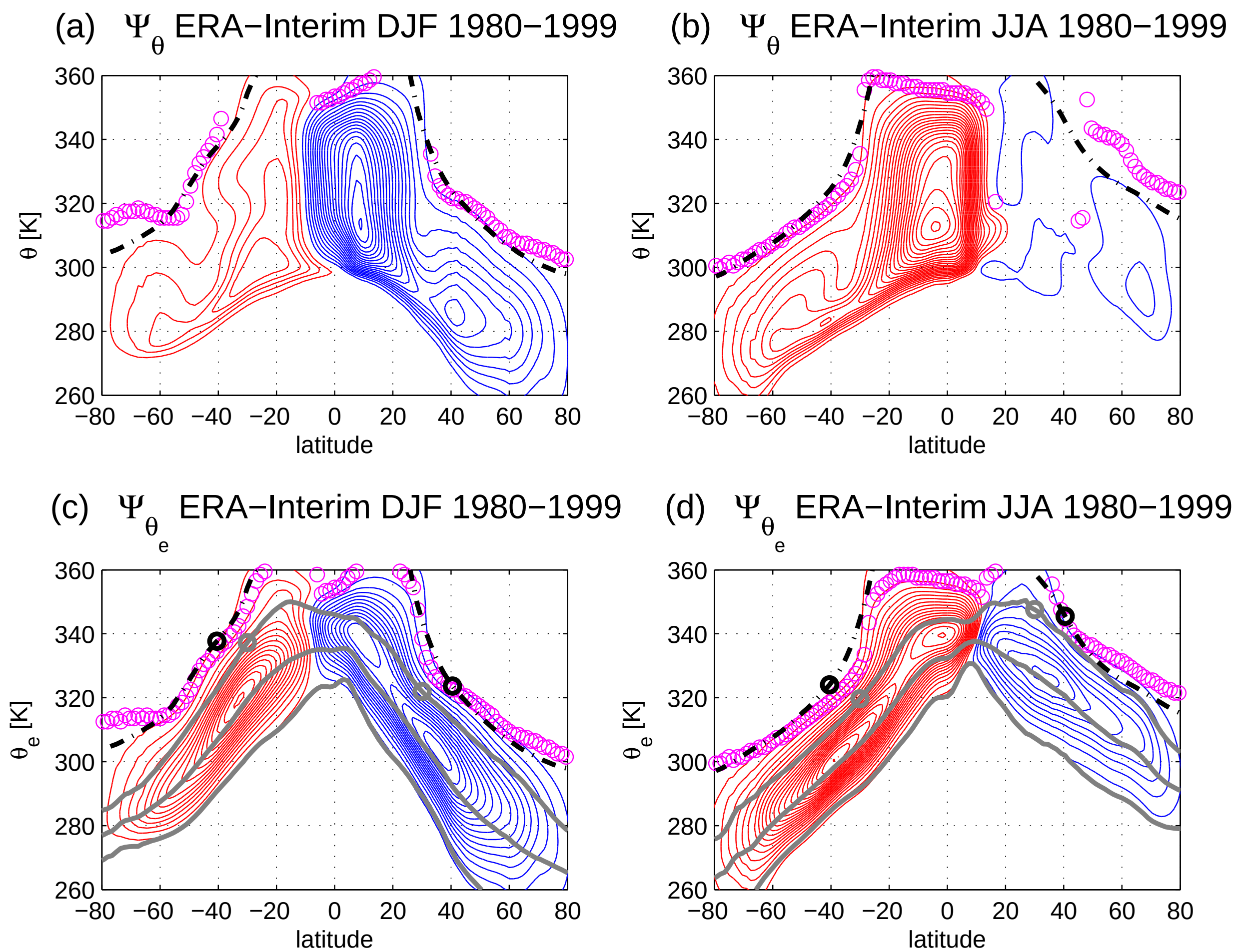


FIG. 1. The climatological streamfunction of the STEM isentropic circulation averaged on (a)(b) dry ($\Psi_{\mathrm{STEM}}(\phi,\theta)$) and (c)(d) moist isentropic surfaces ($\Psi_{\mathrm{STEM}}(\phi,\theta_e)$) for December-January-February (DJF) and June-July-August (JJA) during 1980-1999 using the ERA-Interim Reanalysis dataset. The contour interval for the streamfunction is $1 \times 10^{10}$ kg/s and blue (red) contours represent clockwise (counterclockwise) circulation. The pink circles indicate the 10% of the maximum streamfunction. The thick black dashed-dotted lines show the mean potential temperature at the dynamical tropopause identified as the level of 2 PVU of potential vorticity. The three thick grey lines in (c)(d) represent the mean minus two standard deviations, the mean, and the mean plus two standard deviations of the equivalent potential temperature at 850 mb, respectively. The black circles mark the dynamical tropopause at 40°N(S) and the grey circles denote the mean plus two standard deviations of the equivalent potential temperature at 850 mb at 30°N(S).

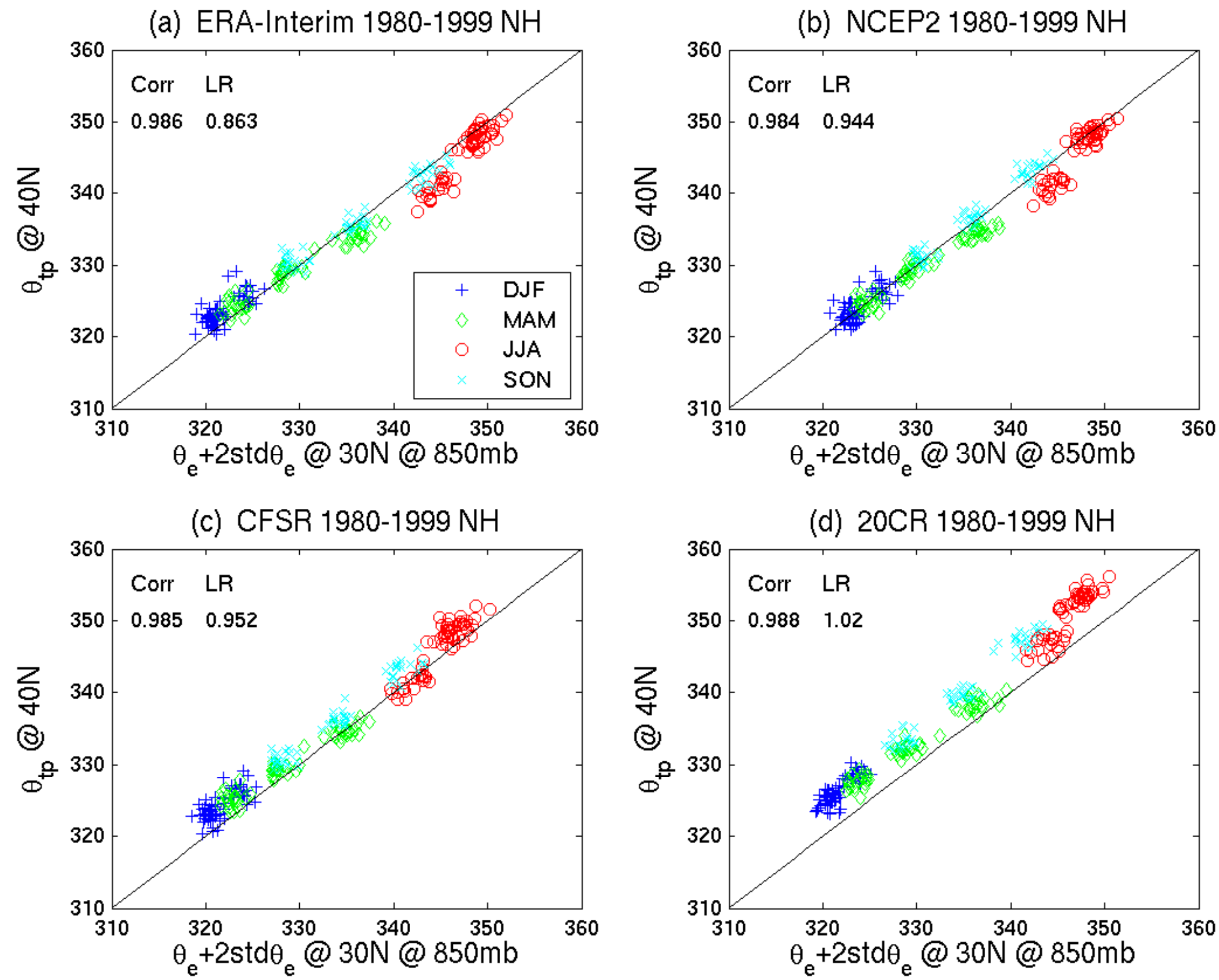


FIG. 2. The annual cycle of the moist dynamical constraint between the 850 mb $\theta_{e,\mathrm{pf}}$ ($= \overline{\theta_e} + 2\overline{\theta_e'^2}^{1/2}$) at 30°N and the mean dynamical tropopause $\theta_{\mathrm{tp}}$ at 40°N for the four reanalysis datasets. The plus symbols correspond to DJF, diamond symbols to March-April-May (MAM), circles to JJA, and crosses to September-October-November (SON), as indicated in legend. The coefficients of correlation and linear regression are also shown.

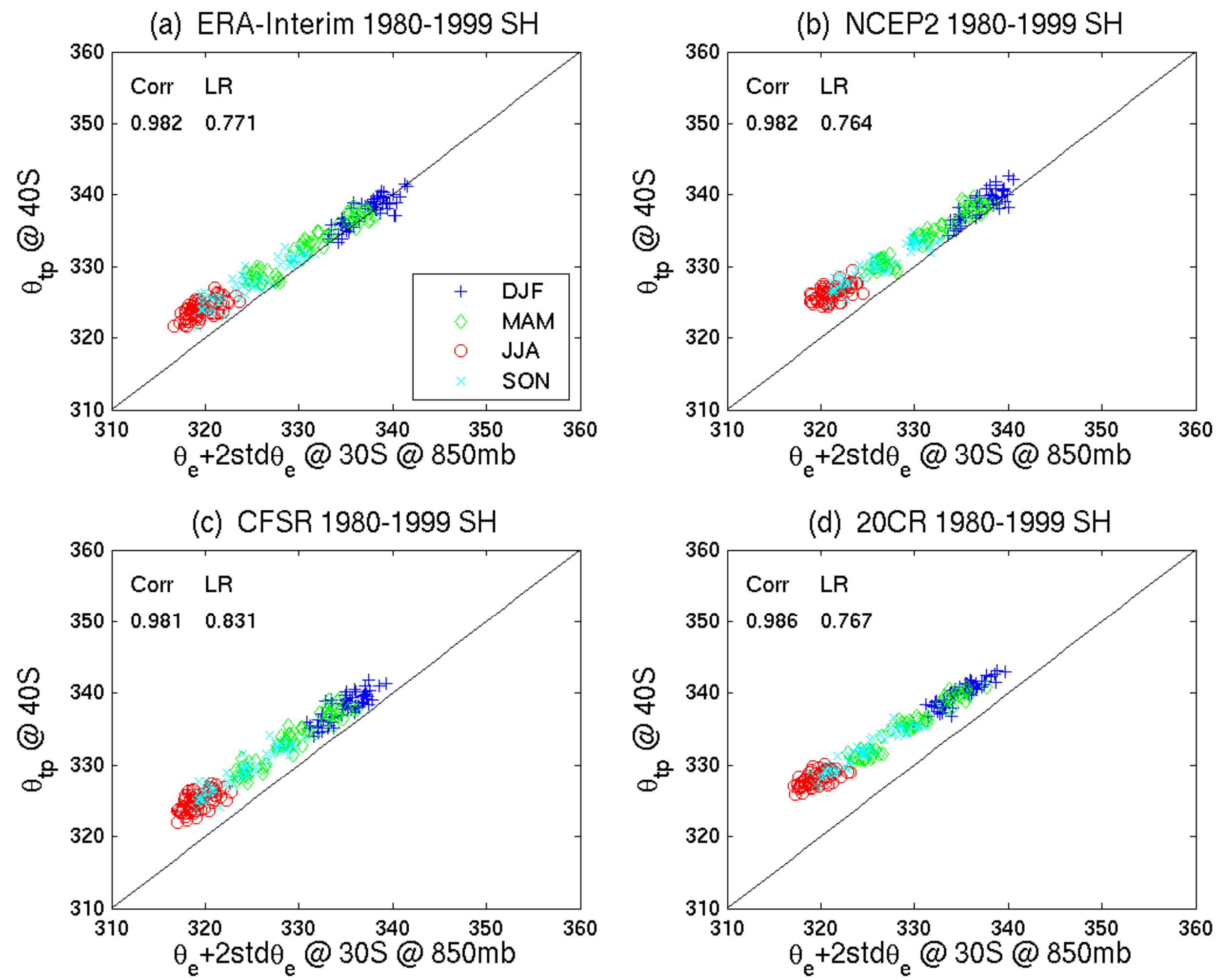


FIG. 3. Same as Figure 2 but for the Southern Hemisphere.

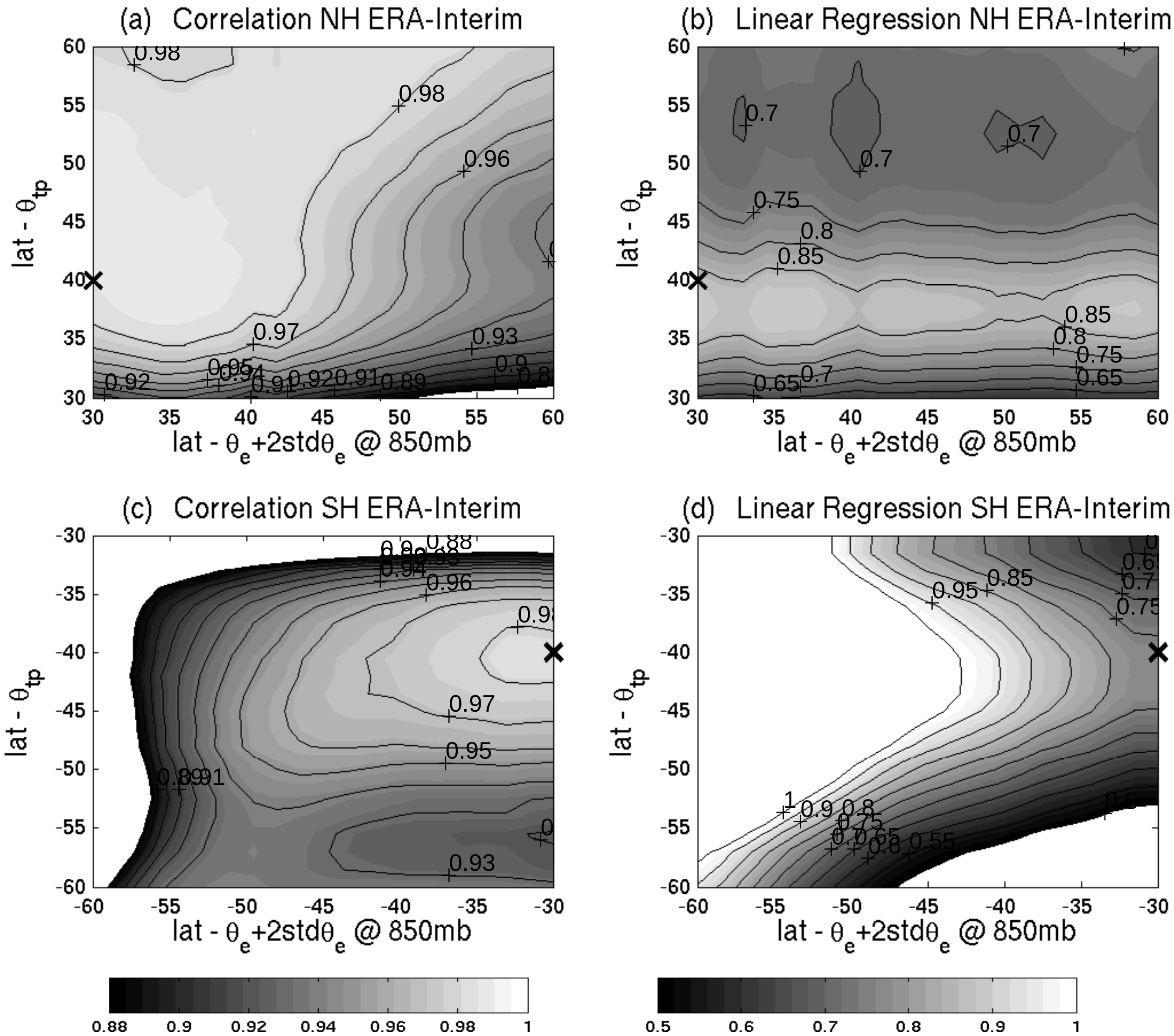


FIG. 4. The coefficients of correlation (left) and linear regression (right) in the annual cycle of the moist dynamical constraint over a range of midlatitudes from 30°N to 60°N (top) and from 60°S to 30°S (bottom) for both $\theta_{e,\mathrm{pf}}$ $(= \overline{\theta_e} + 2\overline{\theta_e'^2}^{1/2})$ at 850 mb and the mean dynamical tropopause $\theta_{\mathrm{tp}}$. Subplots (a)(c) and (b)(d), respectively, share the same color bars.

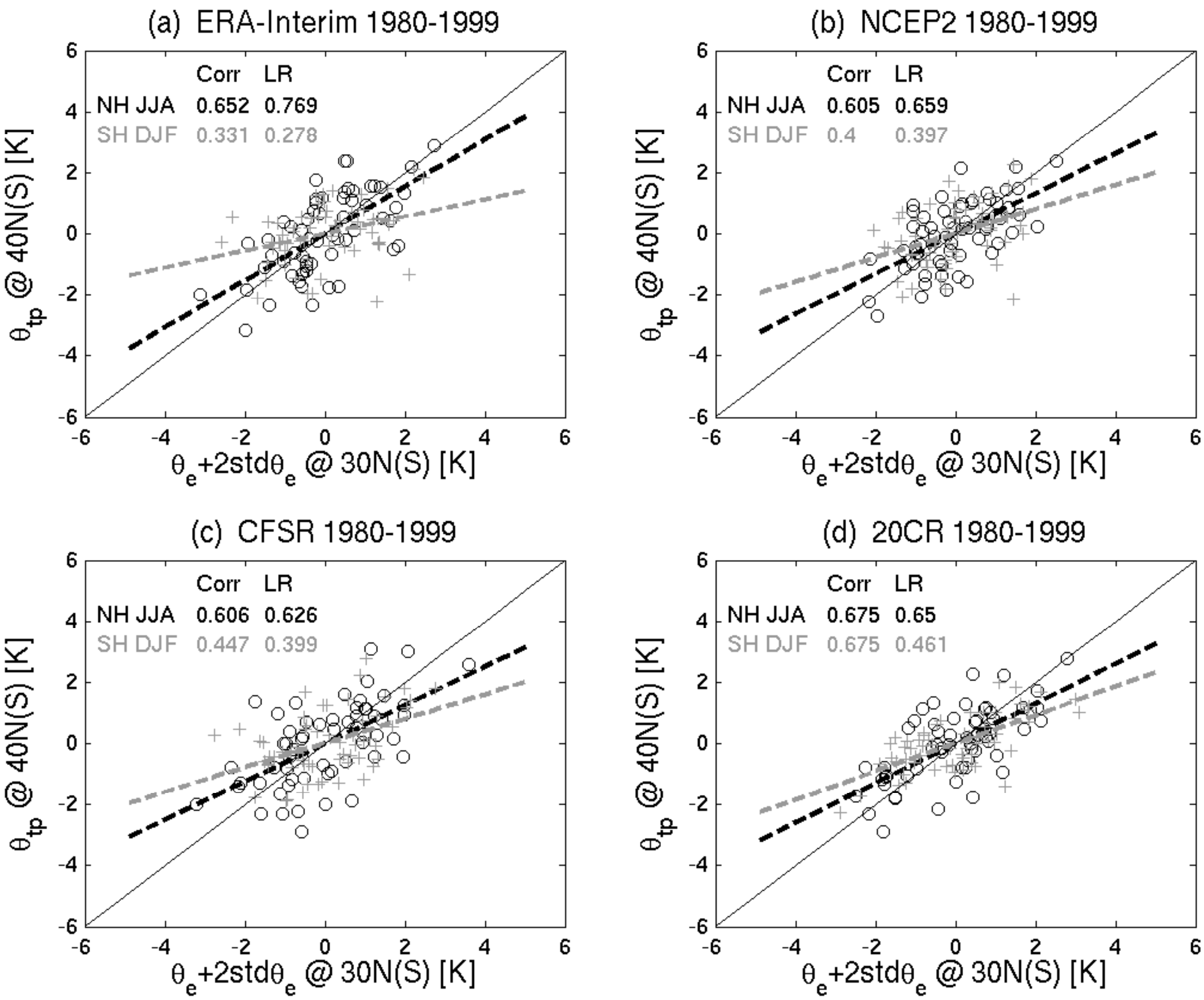


FIG. 5. Same as Figures 2 and 3 but for summer (NH JJA (black symbols) and SH DJF (grey symbols)) monthly anomalies (with climatological monthly averages removed) for the four reanalyses.

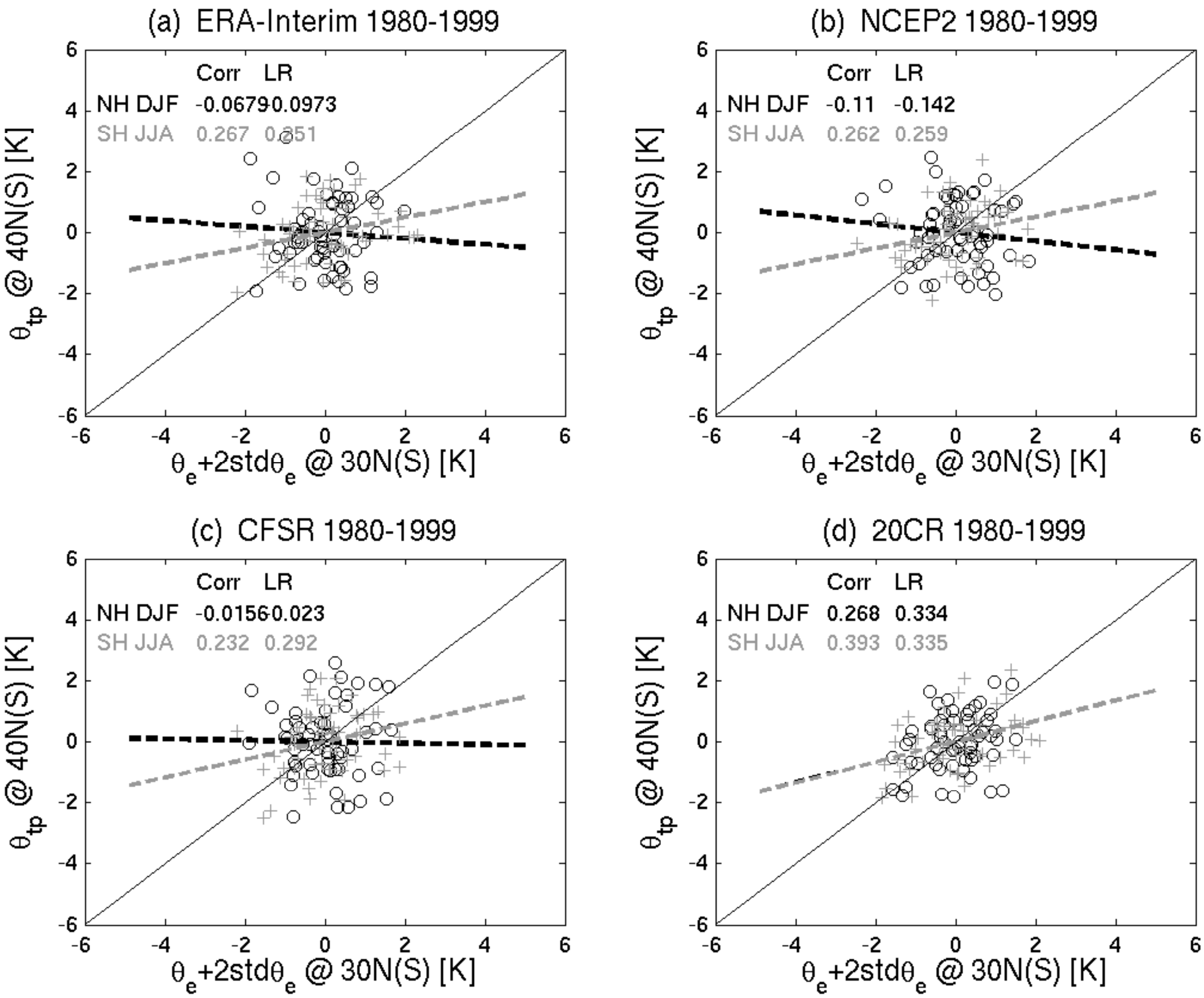


FIG. 6. Same as Figure 5 but for winter (NH DJF (black symbols) and SH JJA (grey symbols)).

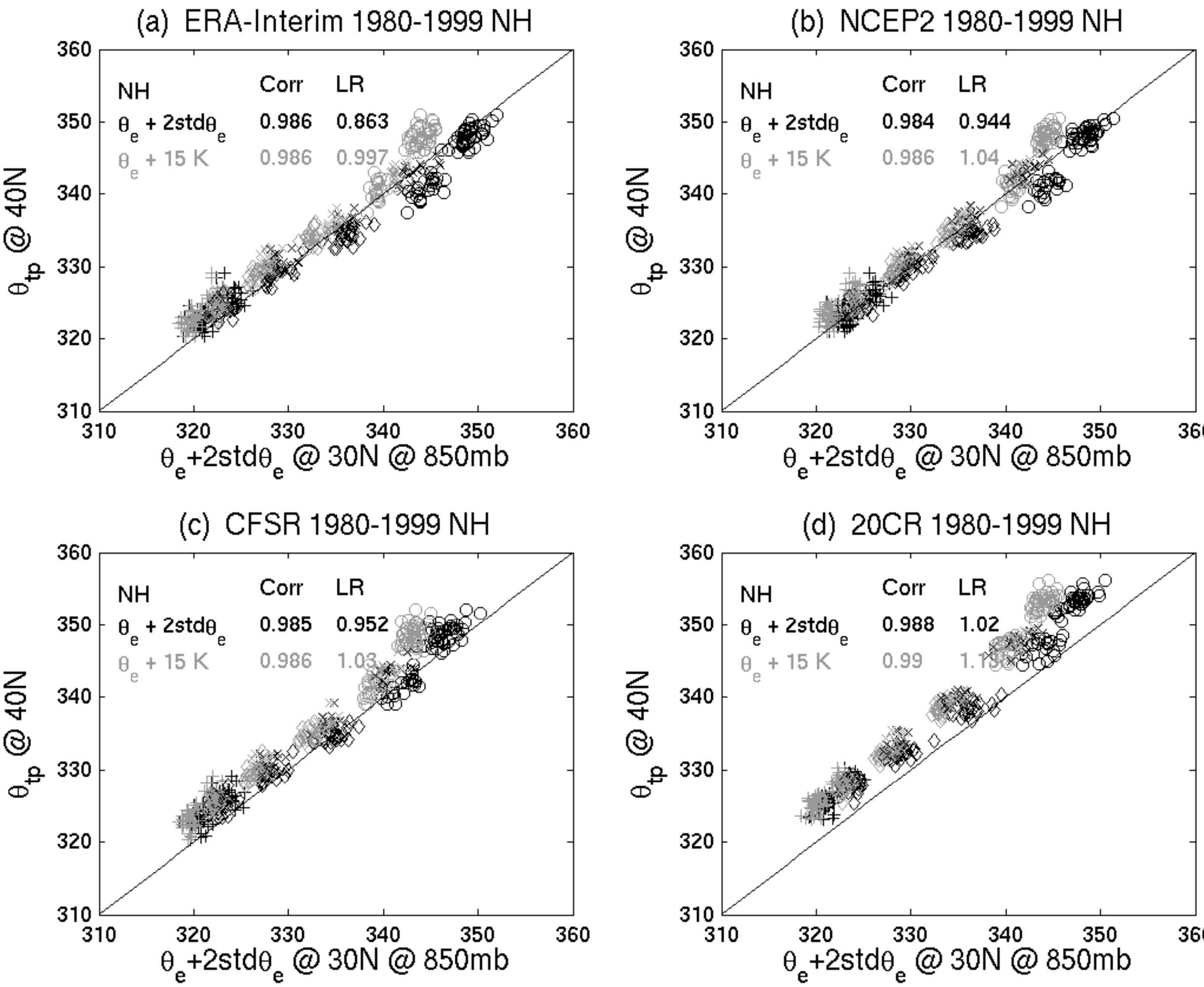


FIG. 7. Same as Figure 2 (black symbols) but in comparison with the annual cycle using the mean value of $\theta_e$ plus a constant value (15 K), in the absence of eddy fluctuations (gray symbols).